2D Arrays of Organic Qubit Candidates Embedded into a Pillared-Paddlewheel Metal-Organic Framework

Marcus J. Jellen,[†,=] Mayokun J. Ayodele,[‡,=] Annabelle Cantu,[†] Malcolm D. E. Forbes,[‡,*] and Miguel A. Garcia–Garibay[†,*]

[†]Department of Chemistry and Biochemistry, University of California, Los Angeles CA 90095–1569 USA

[‡]Department of Chemistry and Center for Photochemical Sciences, Bowling Green State University, Bowling Green, OH 43403–0001 USA

ABSTRACT: The creation of ordered arrays of qubits that can be interfaced from the macroscopic world is an essential challenge for the development of quantum information science (QIS) currently being explored by chemists and physicists. Recently, porous metal-organic frameworks (MOFs) have arisen as a promising solution to this challenge as they allow for atomic-level spatial control of the molecular subunits that comprise their structures. To date, no organic qubit candidates have been installed in MOFs despite their structural variability and promise for creating systems with adjustable properties. With this in mind, we report the development of a pillared-paddlewheel-type MOF structure that contains 4,7–bis(2-(4-pyridyl)-ethynyl) isoindoline N-oxide and 1,4–bis(2-(4-pyridyl)-ethynyl)-benzene pillars that connect 2D sheets of 9,10-dicarboxytriptycene struts and $Zn_2(CO_2)_4$ secondary binding units. The design allows for the formation of ordered arrays of reorienting isoindoline nitroxide spin centers with variable concentrations through the use of mixed crystals containing the secondary 1,4-phenylene pillar. While solvent removal causes decomposition of the MOF, magnetometry measurements of the MOF containing only N-oxide pillars demonstrated magnetic interactions with changes in magnetic moment as a function of temperature between 150 and 5 K. Variable-temperature electron paramagnetic resonance (EPR) experiments show that the nitroxides couple to one another at distances as long as 2 nm, but act independently at distances of 10 nm or more. We also use a specially designed resonance microwave cavity to measure the face-dependent EPR spectra of the crystal, demonstrating that it has anisotropic interactions with impingent electromagnetic radiation.

INTRODUCTION

Quantum information science (QIS) has the potential to revolutionize science and engineering by taking advantage of counterintuitive quantum phenomena, such as entanglements and superpositions of states, that will enable, for example, large–scale applications in quantum computing, quantum sensing, and quantum communications.[1] While current computers utilize classical bits existing in one of two states (0 or 1) in order to carry out computations, quantum bits (qubits) harness the nature of quantum particles, which allows them to exist in a coherent superposition of two or more states and therefore, are able to carry out multiple commands simultaneously.[2] Early examples of qubits include photons,[3] nuclear spins in nitrogen doped diamonds,[4] and superconducting states in Josephson–Junctions.[5] The manipulation of electron spins on molecules using pulsed microwave pulses comprises a relatively new and promising pathway currently being explored in the QIS and magnetic materials fields.[6] Paramagnetic metal centers with "spin free" ligands have already shown tremendous promise for the development of qubits with coherence times up to 150 μs.[7] However, stable organic radicals also comprise a useful subset of potential qubits due to their structural variability and synthetic accessibility, which makes it possible to further engineer them into highly ordered crystalline meta–architectures with multiple functional features,[8] including the opportunity to develop multiscale platforms to transduce molecular and supramolecular properties into the macroscopic world.[9,10]

The first challenge of the organic approach comes from the great difficulties related to the predictability and limited functionality of close packed molecular crystals. Insight from reticular chemistry offers promising solutions toward the creation of ordered arrays of organic qubits through the use of metal-organic frameworks (MOFs). MOFs are porous materials comprised of inorganic nodes connected by organic linkers. Careful selection of the metal and organic building blocks allows structures with variable geometries and engineered molecular dynamics to be constructed in a predictable fashion.[9] This control over structure will allow for the precise placement of qubits with predetermined distances and orientations with respect to one another, with additional degrees of freedom available by switching between alternative orientations.[10] Well-characterized MOF structures containing static qubits are reported in the literature, in particular those using tetracarboxy porphyrin linkers.[11] These studies show the power of reticular chemistry for the advancement of QIS by establishing a 50 Å coupling limit between neighboring qubits,[12] as well as developing qubits that maintain their coherence for up

to 14 μs[13] and the preservation of spin coherence at room temperature[14] using Cu(II), Co(II) or VO(IV) metal centers, respectively. However, relatively few examples of MOFs with paramagnetic centers on organic linkers are known in the literature as compared to their inorganic counterparts.[15]

Here we describe the synthesis and characterization of **UCLA-NO/Ph**, a multi-component pillared paddlewheel metal organic framework (Scheme 1) with paramagnetic isoindoline–N–Oxide rotors **1**, and diamagnetic 1,4–bis(2-(4-pyridyl)-ethynyl)-benzene, **2**, linkers. These ligands connect impenetrable 2–D sheets composed of $Zn_2(CO_2)_4$ secondary binding units (SBUs), **3**, which are composed of Zn^{2+} metal clusters and 9,10–dicarboxytriptycene struts, **4**. The diamagnetic phenylene linker **2** was chosen as an isostructural ligand to prepare magnetically diluted mixed crystalline samples of **UCLA–NO/Ph**, which maintain the original lattice geometry.

Scheme 1

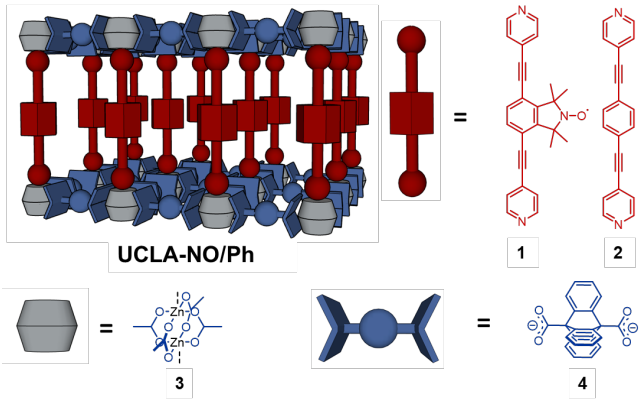

Our design has a few key features worth noting. A lattice constant of *ca*. 10 Å can accommodate molecular rotors with a radius of revolution of ca. 7 Å, making it possible for a nitroxide radical to rotate and reorient without having to overcome steric barriers. Furthermore, the nitroxide–bearing moiety is suspended between two alkynes, which are known to have a vanishingly low intrinsic activation barrier for axial rotation.[9] In the absence of solvent, these features would allow the crystalline rotators to reorient, even at cryogenic temperatures (10 K or below),[16] such that it would be possible to use external electric fields to affect the macroscopic polarization[10,17] arising from the collective interactions of the nitroxide electric dipole moments. Under these conditions, electric fields may be used to alter magnetic order and QIS properties, including the potential of encoding information within the shapes of standing microwave cavity modes, and controlling the transmission of magnetic information along rotary dipole chains.[18] As a new class of organic multiferroic materials with tetragonal order, these systems would have the potential of undergoing spontaneous dipole–dipole–induced anti–ferromagnetic (AF) transitions at the Néel temperature to create chains of spin–paired nitroxides.[19] Furthermore, the layered tetragonal nature of **UCLA–NO** not only insulates the nitroxide rotors between the 2D-nets formed by **3** and **4**, but it also allows for the application of transverse magnetic fields along specific crystallographic faces of the MOF. Such features are vital for the transmission of classical information along well-defined crystal axes.[20] And finally, the formation of mixed crystals utilizing diamagnetic moiety **2** to dilute the spin concentration will make it possible to study temperature– and concentration–dependent anisotropic exchange interactions with electron paramagnetic resonance (EPR) spectroscopy.

RESULTS AND DISCUSSION

Synthesis. Nitroxide rotor **1** was synthesized via a modified procedure developed by Kitagawa and coworkers.[21] The key Sonogashira coupling reaction is illustrated in Scheme **2**. After much tribulation, we discovered that this coupling only proceeds in pure tetramethylpyridine as the solvent. Single crystals, suitable for X–ray analysis, were grown from a super–saturated solution of **1** in ethanol. The other **UCLA–NO** components **2** and **4** were synthesized according to literature methods, with slight modifications, (see SI).[22]

Scheme 2

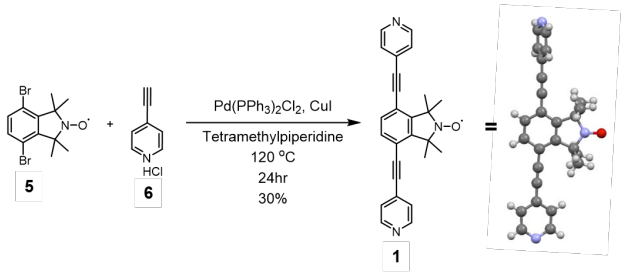

Finally, samples of the new MOF **UCLA–NO** were prepared via a convenient solvothermal synthesis in DMF.[23] All MOF components were added to a 10 mL vial, covered in 3.0 mL of anhydrous DMF and then placed in an oven overnight at 100 °C. Diluted samples were prepared by using the appropriate molar ratio of **1**:**2** in the solvothermal synthesis. Samples of **UCLA–NO** showed decomposition when heated under vacuum to remove solvent (Figure S9 and S10) and upon mechanical grinding. We attribute this sensitivity to the weak dative bond between pyridine and zinc, as well as the flexible alkyne linker, which is prone to displacement by water.[24] Flattened rectangular prismatic crystals amenable to pan–powder X–ray diffraction (PXRD) were washed with fresh DMF before further investigation.

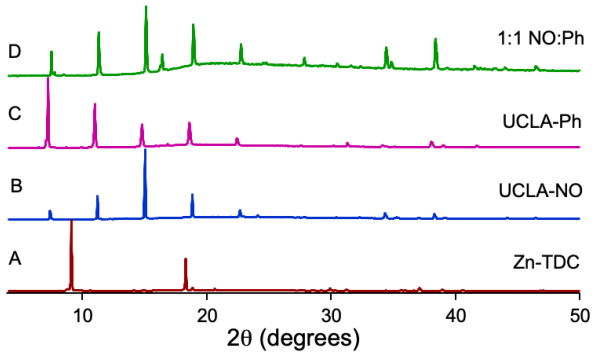

Figure 1. PXRD traces of A) Zn–TDC crystals, B) **UCLA–NO**, C) **UCLA–Ph**, D) 1:1 Diluted **UCLA–NO**.

X-ray Crystallography. The PXRD analyses were carried out with Cu–Kα1 radiation (1.5406 Å). Samples were placed on a zero–background plate at a fixed stage with a drop of DMF to prevent crystal collapse by desolvation. Data was collected from 2 theta angles of 5 to 50 degrees at room tem-

perature. The step width was 0.016 degrees, with the acquisition time being approximately 10 s at each step. We first analyzed crystals composed of only **3** and **4** as a control (Figure 1A) followed by analysis of crystals obtained with the addition of pillars **1**, and/or **2**. Crystals with 100% pillar **1** or **2** are shown in Figures 1B and 1C, respectively, which confirm the formation of two isostructural crystal lattices. Crystals prepared with a 50:50 mixture of **1** and **2** demonstrated that the two pillars are able to form substitutional isoreticular solid solutions that make it possible to dilute the nitroxide radical (Figure 1D) throughout the MOF structure. Analysis of the crystal structure of **UCLA–NO** and **UCLA–Ph** shows that the distance between layers are slightly wider in the case of **UCLA–NO** (20.492 Å vs. 20.364 Å), explaining the slight shift to lower angles for UCLA–**Ph** (Figure S13 and S14). Additionally, the broad peak from 15 to 30 degrees in figure 1D, and to a lesser extent, 1C and 1B, are attributed to the presence of included solvent.

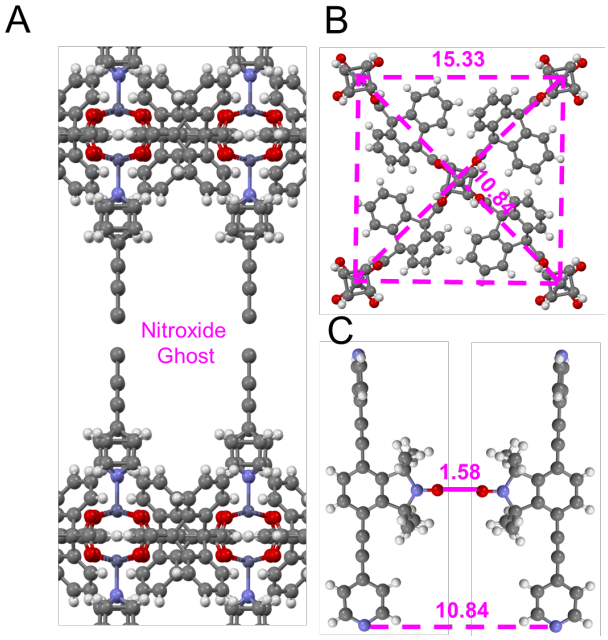

Figure 2. A) Crystal structure of **UCLA–NO** displaying no nitroxide rotator. B) Distance analysis between pillar agents in the MOF. C) Distance between head–to–head nitroxide oxygen rotors (distances in Å).

Single crystal X-ray diffraction data measured with Cu–Kα radiation (λ = 1.5046 Å) were obtained from a solvent–containing yellow crystal of **UCLA–NO**. Diffraction patterns were collected at 200 K with an area detector and the structure solved and refined with the SHELXTL program. While all heavy atoms were refined anisotropically, the hydrogen atoms were placed at the calculated positions. The diffraction data were solved in the tetragonal space group p4/mbm with a modest Rf= 6.05%. Unit cell dimensions a = 15.3316(6) and b = 15.3316(6) are equivalent and shorter than c = 23.4500(13) by approximately 8.11 Å. All angles are equal to the expected tetragonal angle of 90°. Two notable features of the structure are 1) the rotationally disordered pyridyl groups occupying positions related by 90°, and 2) the "missing" nitroxide radical, indicating that it has no preferred orientation, as expected for a group that can undergo diffusional rotation (Figure 2A). Further analysis of the structure shows that neighboring pillars are approximately 10.84 Å apart (Figure 2B), and using simple models and geometric considerations one can determine that the closest head–to–head distance between neighboring nitroxides would have oxygen-oxygen distances of ca. 1.58 Å (Figure 2C). While this distance is shorter than the Van der Waal radii of the two oxygen atoms (3.04 Å), and on the order of a peroxide O–O single bond (ca. 1.45 Å), a bond is not expected in this case due to unfavorable energetics and steric interactions. However, this observation suggests the potential of reaching configurations where neighboring radicals may have strong magnetic dipole and exchange interactions. In fact, antiferromagnetic coupling of neighboring N–O functional groups has been observed in adamantly nitroxide plastic crystals at temperatures as low as 1.48 K, when the N–O to N–O distances are ca. 4 Å apart,[18] and as high as 260 K when antiparallel N-O dimers can be formed with intermolecular N···O distances of ca. 2.2 Å.[25]

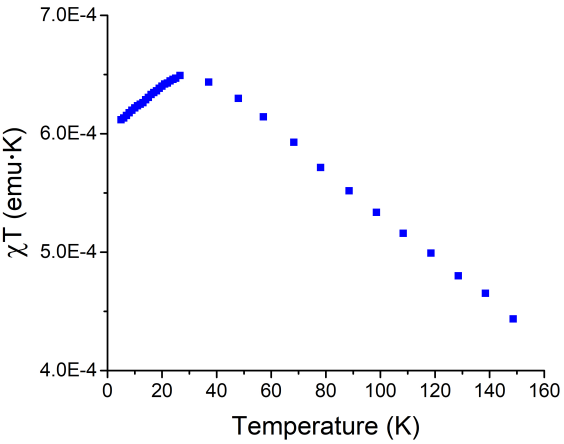

Figure 3. Zero-field cooling of **UCLA–NO** from 150 K to 5 K illustrating the temperature dependence of χT.

The possibility of observing intermolecular magnetic interactions was examined by measuring the temperature dependence of the magnetic susceptibility ($\chi_{(T)}$) using a superconducting quantum interference device (SQUID) magnetometer. While paramagnetic samples display magnetic susceptibilities with a temperature dependence characterized by an Arrhenius behavior, a sharp increase at the Curie temperature is observed for ferromagnetic materials, and a sharp decrease for antiferromagnetic materials is observed at the analogous Neel temperature.[26] Samples of **UCLA–NO** were sealed in a quartz tube under a 700 torr vacuum with a small amount of solvent in order to prevent MOF decomposition. Zero–field cooling (ZFC) results suggest at first sight a typical Arrhenius-type behavior at all temperatures ranging from 150 K to 5 K (Figure S15). However, a plot of $\chi_{(T)}$T vs. T (Figure 3) shows that $\chi_{(T)}$T gradually increases until it reaches a maximum value at ca. 30 K. After this point, $\chi_{(T)}$T begins to decrease until 5 K, the lowest temperature in the measurement. While proper diamagnetic corrections were not feasible with this sample due to the included solvent, the observation that $\chi_{(T)}$T increases by 1.5 times its initial value before decreasing once again is indicative of weak high spin and pairing interactions between

neighboring isoindoline nitroxides.[27] Similar field-cooled (FC) measurements carried out at 5000 Oe exhibited a much more dramatic slope, due to the increased external field, but also shows a slight curving below 30 K, demonstrating that these coupling interactions are not blocked by increased magnetic fields (Figure S15). A field–dependent measurements of 100% **UCLA–NO** run at 7 K exhibited no hysteresis, demonstrating that the interactions leading to this change in $\chi_{(T)}T$ are either very weak or arise from very few interacting partners at this temperature (Figure S15). EPR data below revealed traces of Cu(II) ions in sample, but we are currently unable for account for them in the magnetometry data.

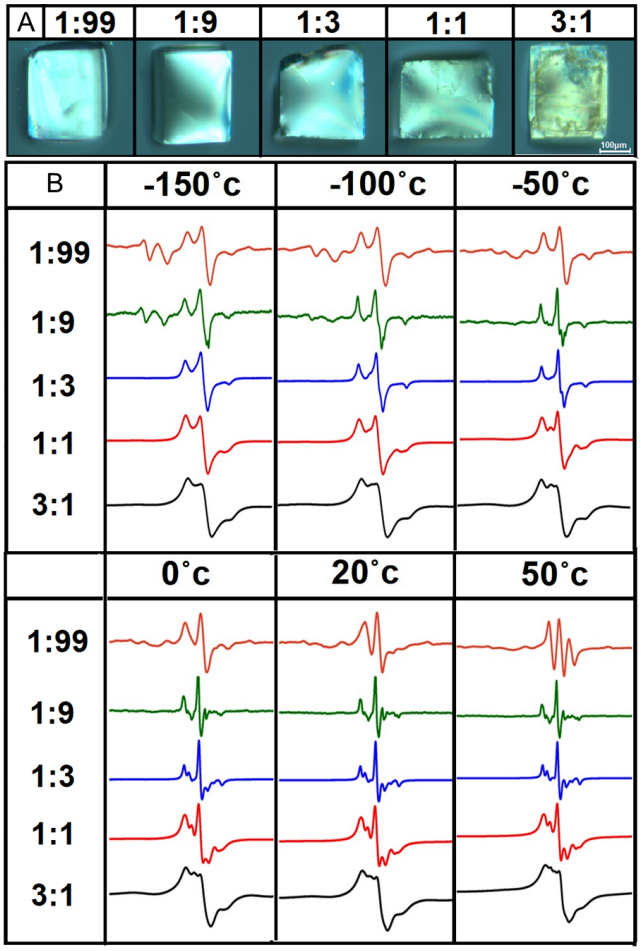

Figure 3. A) Single crystal photos of the nitroxide MOFs in this study at ambient conditions. B) Variable temperature EPR measurements ranging from –150 °C to 50 °C of **UCLA–NO** mixed crystals with various concentrations of **1:2**.

Variable-Temperature EPR Analysis. Wet crystals of the nitroxide–containing MOF were filtered and immediately inserted into a quartz capillary tube, and sealed at both ends. The sealed tube was then placed into a JEOL EPR resonant cavity (TE_{011}) connected with a liquid nitrogen dewar system. Steady state electron paramagnetic resonance (SSEPR) experiments were carried out at different temperatures ranging from –150 °C to +50 °C using a sweep width of 50 mT and a 100 kHz modulation amplitude of 0.1 mT, except for the 1:99 diluted Nitroxide MOF, for which 0.8 mT modulation amplitude was used. We collected EPR data for **UCLA–NO** (Figure S16) and the following additional nitroxide MOFs with varying compositions of nitroxide to phenylene pillars (**1**:**2**) equaling 3:1, 1:1,1:3, 1:9, and 1:99, respectively (Figure 3).

At 50 °C, only the most diluted nitroxide MOF 1:99 showed the complete three-line spectra expected for an isolated nitroxide radical as a result of hyperfine coupling interactions with the ^{14}N nitrogen nucleus, which has a total nuclear spin **I** = 1. At this high temperature, the isoindoline nitroxide radical would have the freedom to rapidly reorient about its axis, with an activation barrier determined by the solvent occluded within the pores of MOF. As the temperature decreases from 50 °C to –150 °C, the nitroxide radical experiences increasingly slower rotation, with longer rotational correlation times that result in spectral broadening. In fact, an increase in line broadening is observed in the spectra for all the MOF compositions. Two additional peaks observed at low field in the lower temperature spectra (–50 °C to –150 °C) for the 1:99 and 1:9 ratio samples are assigned to residual copper (II) ions, which are found as trace impurities in the synthesis.[28] These signals did not appear in the 3:1, 1:1 and 1:3 samples where the nitroxide radicals are present in much higher concentration. Moving from top to bottom in Figure 3B as the samples change from low to high nitroxide concentrations, the spectra become increasingly broadened. This broadening is due to Heisenberg spin exchange as neighboring electrons with identical spin states are close enough to swap their spin information at a rate that is much faster than the rate of the inverse of the hyperfine interactions.[29] In going from lower to higher temperatures at intermediate concentrations, the line shapes sharpen at higher temperatures as a result of motional narrowing.

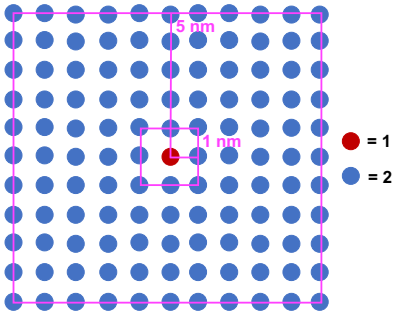

Figure 4. Schematic representation of the MOF layer indicating the average distances between a nitroxide pillar at the center for **1:2**=1:9 (center square, d_{ave}≈2 nm) and **1:2**=1:99 dilutions (outer square, d_{ave} ≈ 10 nm).

The extent of through-space exchange and dipole-dipole radical–radical interactions between nitroxides in the layers will depend on their distance (d_{RR}). Assuming the formation of a random solid solution, the average value d_{RRave} should be statistically determined by the nitroxide concentration. For example, a nitroxide in a 1:99 sample (represented with a red dot in the 10 x 10 array in Figure 4), will be surrounded by phenylene pillars **2** (blue dots). One may expect that their nearest next neighbors will be on average *ca*. 10 nm away with others at shorter and longer distances with varying probabilities. However, at dilutions 1:9 and lower, one may expect that

there will be a significant fraction of nitroxides within closest neighboring distances of ca. 1 nm and 1.4 nm. We assume that radical–radical interactions occurring among layers along the crystal c axis will not be significant. Our results indicate that nitroxides begin to lose communication when they are on average ca. 2 nm apart, and they behave as independent mono-radicals at a separation of about 10 nm. Similar limits have been experimentally observed for both electron–nuclear spin dipolar interactions and electron–electron exchange interactions.[30] This finding demonstrates that the nitroxide rotors in this structure may be sensitive to both environmental changes and to paramagnetic impurities.

Figure 5. Single–crystal EPR measurements of a **1**:**1** diluted crystal of **UCLA–NO** analyzing each orientation of the crystal from 0° to 330° in 30° increments.

Single-Crystal EPR Analysis. Further EPR analyses were carried out on a single crystal of the 1:1 diluted nitroxide using a specially designed microwave resonator that allowed for coarse crystal rotations, to explore the angular dependence of the applied external magnetic field. A 200 x 150 x 100 μm sized single crystal shaped as a flattened cuboid was selected, covered with mineral oil, and placed on a microscope slide that was inserted and held rigid in the center of an JEOL EPR wafer cavity (TM_{110}), specially designed for solid and flat samples.

The starting position for the crystal rotation was arbitrary, but to define a laboratory frame of reference, an arbitrary x–axis was chosen to lie along the longer side of the crystal and parallel to the surface of the sample holder, but perpendicular to the direction of the magnetic field that aligns with a relative z–axis of the crystal. The crystal was then flipped to an upright position making a new, relative, y–axis lie along the sample holder while the initial x–axis now perpendicular to both sample holder plane and magnetic field direction. Finally, the crystal was tilted sideways about the y–axis such that it remains parallel to the sample holder plane and places the arbitrary z–axis perpendicular to the magnetic field. Experiments were carried out at 30° rotation intervals over a 360° rotation with each axis aligned with the sample holder plane under ambient conditions. A sweep width of 20 mT and a modulation amplitude of 1.0 mT were used for each 4–minute scan.

Close analyses of the dataset in Figure 5 shows that the spectra obtained by rotation along the y and z axes are similar, but inversed (starting with angle 30° of z is the same as starting at angle 330° of y). However, rotation about the x axis yields distinct spectra. We know that in many cases, the crystal habit approaches the symmetry of the unit cell. Based on this data, we conclude that rotation about the x axis of the laboratory frame reflects rotation about the approximate 4–fold symmetry axis of the crystal, which is a unique axis and lies along the shorter edge of the crystal as illustrated in Figure 6. This observation is confirmed as the spectra repeats at 90° intervals. Rotation along the y and z axis is similar and their spectra repeat at 10° intervals, indicating that they are the crystallographic 2–fold axes. These both lie along the longer edges of the crystal.

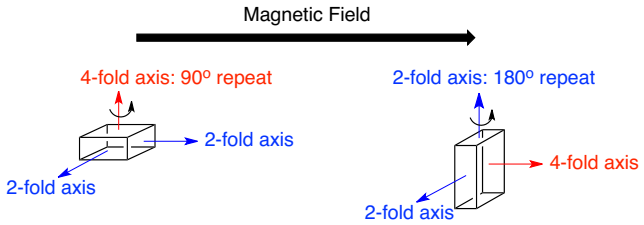

Figure 6. Rotational symmetry of crystal sample placed in the EPR cavity.

As expected for a low density amphidynamic crystal with a static frame linked to axially rotating radicals, the EPR spectra of **UCLA-NO** were not characterized by a single sharp line due to exchange narrowing, as it is commonly observed in close packed crystalline nitroxides such as crystals of pure pillar **1** (Figure S17). By contrast, one can see broadened

three–line spectra determined of the hyperfine splitting of the radical with the ^{14}N nucleus with **I** = 1. An additional set of peaks are apparent in both the low field and mid field signals of all three axes at angles; 0°, 30°, 90°, 150°, 180°, 210°, 270°, 300°, and 330°, suggesting that there are two or more populations of nitroxides within the MOF cavity that have different chemical environments. Interestingly, the high field line of these signals shows a broadening effect not present in the other two resonances, as expected from the cumulative effect of the field-dependent g-factor and A (hyperfine coupling) anisotropies (tensors). These two non–equivalent nitroxide types might be due to the slight deviation from tetragonal packing in the crystal structure, which is reduced to the monoclinic space group C2/c. This would cause different orientations of the $2p_z$ orbital of the N atom to exist relative to the crystal frame, but not relative to the symmetric molecular backbone. It is good to bear in mind that we are dealing with pillared MOFs in which we have a 2–D framework joined together by an orthogonal pillar linker with the attached nitroxide (Figure 7). This means that the molecular rotation is restricted to one degree of freedom and along one of the crystallographic axes. Along the x–axis dataset, there is overlap of split peaks at 30°, 60°, 120°, 150°, 210°, 240°, 300° and 330° which suggests the two inequivalent nitroxides might experience similar positioning at these angles.

Furthermore, it can be observed in both the y and z datasets that the hyperfine splitting changes significantly, as judged by the spacing between the three lines. Spectra at 90° and 270° show the smallest hyperfine splitting, while the largest splitting is observed at 0° and 180°. By contrast, the hyperfine splitting on the spectra along the x–axis is relatively constant, suggesting that internal rotation of the nitroxide partly averages its anisotropy by sampling all orientations along the y-z plane. With the molecular frame indicated in capital bold letters, we define the ***Z***–axis along the $2p_z$ orbital of the N–O bond. While it is common to define the molecular x-axis along the direction of the N-O bond vector, for convenience we will assume that the direction of the molecular ***X***–axis coincides with that of the laboratory x-axis, which corresponds to the axis of rotation along C2 and C5 of the benzene ring (Figure 7). In this coordinate system, the N-O bond vector along the molecular ***Y***-axis can occupy all possible orientations in the laboratory y-z plane.[31]

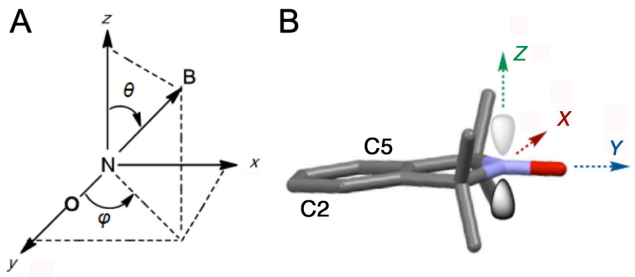

Figure 7. A) Nitroxide molecular coordinate and spherical coordinates defining the direction of external magnetic field. B) The nitroxide ring with a defined molecular frame: z (green), x (orange) and y (blue).

Having described the relation between molecular and laboratory frames of reference, we can analyze the spectra shown in Figure 5 and draw general conclusions on the anisotropy of the hyperfine splitting. We can see that rotation about the laboratory four–fold x axis leads to a relatively constant hyperfine interaction, as revealed by the spacing of the three lines and the spectral amplitude. This is consistent with the fact that the nitroxide bond vector along the molecular *Y* axis can occupy all possible orientations in the laboratory y–z plane. This causes the hyperfine constant to become isotropic with respect to rotation about this axis. By contrast, rotation about the laboratory y and z axes modulates the orientation of the nitroxide p-orbital and the N-O bond vector between parallel and perpendicular orientations with respect to the direction of the magnetic field. Based on these observations, we propose that the smallest hyperfine splitting is obtained when the direction of the N-O bond vector (molecular ***Y***-axis) is orthogonal to the external magnetic field, while the largest splitting is observed when the magnetic field is in the orthogonal direction. This is consistent with a hyperfine splitting tensor where the principal components have values in the order $A_{YY} > A_{XX} \approx A_{ZZ}$, as the majority of the electron density is distributed in molecular orbitals parallel to the molecular ***Z***-axis. Therefore, dipole-dipole interactions between the electrons and the proximate nuclei are greatest when the largest components of g and A tensors of the nitroxide are parallel to the N–O bond.

Similar observations have been reported in inclusion crystals of di-tert-butyl-aminyloxyl (di-tert-butyl-nitroxide) and 2,2,6,6-tetramethyl-1-piperidinyloxyl (TEMPO) in hexagonal channels of thiourea and tris(o-pheneylenedioxy)cyclotriphosphazene (TPP).[32] Long needle–like crystals with hexagonal 1–D channels hosting the non–bonded nitroxides were shown to support isotropic rotation about the channel direction in a molecular orientation that places the N-O bond orthogonal to the channel (i.e., rotation about the molecular ***Z*** axis in the molecular frame in Figure 7). It was shown that hyperfine splitting measured with the magnetic field aligned with the needle axis (orthogonal to the N-O bond) was small, and also isotropic as a result of fast rotation. Accordingly, hyperfine splitting measured with the magnetic field orthogonal to the needle axis (i.e., aligned with the N-O bond) is larger and angular dependent. Thus, in agreement with our conclusions and with reference to the molecular frame defined in Figure 7, these studies indicate that $A_{YY} > A_{XX} \approx A_{ZZ}$. Although complications to determine the rotational dynamics in the case of **UCLA–NO** arise from the fact that the solvent causes the rotational motion to be diffusion-controlled, the amphidynamic MOF structure retains the properties of an ordered crystal. Furthermore, we observe significant spin–spin exchange interaction when the neighboring pillars are separated from each other by the lattice constant of ~10.8Å, especially when one considers rotational configurations leading to nitroxide O atoms separated from each other by as little as 1.56 Å, as seen in Figure 2. However, spin exchange decreases as the spins are placed farther away from each other in mixed crystals grown with the diamagnetic phenylene ligands (**2**).

CONCLUSIONS

In conclusion, we have described the preparation and characterization of a layered MOF structure built with nitroxide pillars as a starting point for the generation of crystalline arrays of organic qubits. SQUID magnetometry revealed that the MOF structure containing 100 % N-oxide pillars experienced an effective increase in magnetic moment from 150 K

down to 30K, at which point begun to decrease, suggesting the temperature-mediated population of high spin and pairing interactions between adjacent nitroxides. Using VT EPR spectroscopy we have shown that magnetic interactions display strong anisotropies with impingent electromagnetic radiation, while exchange interactions can be modulated by changes in the nitroxide concentration in diluted crystals prepared with a diamagnetic pillar analog. Our results suggest that these systems will be useful for future QIS applications that will require information to be passed along specific directions of a bulk material while providing a chemical interface for read/write actions. Studies in progress include spectral simulations to explore the dynamics of internal rotation and the development of structures where the solvent can be removed to explore the formation of magnetically ordered phases arising from rotationally ordered states.

ASSOCIATED CONTENT

Supporting Information

Synthesis, characterization, PXRD and EPR spectral data of **UCLA-NO** (PDF). X-ray diffraction data from pillar **1** and from MOF samples **UCLA-NO** and **UCLA-Ph** (cif). Magnetometer measurements of **UCLA-NO** derivatives. The Supporting Information is available free of charge on the ACS Publications website.

AUTHOR INFORMATION

Corresponding Author

* E-mail: forbesm@bgsu.edu
* E-mail: mgg@chem.ucla.edu

Author Contributions

= These authors contributed equally

Funding Sources

MDEF: National Science Foundation award CHE-1900541.
MAGG: National Science Foundation award DMR-1700471

Notes

The authors declare no competing financial interest.

ACKNOWLEDGMENT

MDEF thanks the U.S. National Science Foundation for continued strong support of his research program through grant CHE-1900541. Work at UCLA was supported by National Science Foundation grant DMR-1700471.

REFERENCES

1 (a) Ladd, T. D.; Laflamme, R.; Nakamura, Y.; Monroe, C.; O'Brien, J. L. Quantum Computers. *Nature* **2010**, *464*, 45-53 (b) Kassal, I.; Whitfield, J. D.; Perdomo-Ortiz, A.; Yung, M.-H.; Aspuru-Guzik, A. Simulating Chemistry Using Quantum Computers. *Annu. Rev. Phys. Chem.* **2011**, *62*, 185-207. (c) Simmons, S.; Brown, R. M.; Riemann, H.; Abrosimov, N. V.; Becker, P.; Pohl, H.-J.; Thewalt, M. L. W.; Itoh, K. M.; Morton, J. J. L. Entanglement in a Solid-State Spin Ensemble. *Nature* **2011**, *470*, 69–72. (d) Lanyon, B. P.; Whitfield, J. D.; Gillett, G. G.; Goggin, M. E.; Almeida, M. P.; Kassal, I.; Biamonte, J. D.; Mohseni, M.; Powell, B. J.; Barbieri, M.; Aspuru-Guzik, A.; White, A. G. Towards Quantum Chemistry on a Quantum Computer. *Nature Chem.* **2010**, *2*, 106–111. (e) Degen, C. L.; Reinhard, F.; Cappellaro, P. Quantum Sensing. *Rev. Mod. Phys.* **2017**, *89*, 035002.

2 (a) DiVincenzo, D. P. The Physical Implementation of Quantum Computation. *Fortschritte der Physik* **2000**, *48*, 771–783. (b) Ladd, T. D.; Jelezko, F.; Laflamme, R.; Nakamura, Y.; Monroe, C.; Brien, J. L. O. Quantum Computers. *Nature* **2010**, *464*, 45–53.

3 Chuang I. L.; Yamamoto Y. Spin Quantum Computer. *Phys. Rev. A: At., Mol., Opt. Phys.* **1995**, *52*, 3489–3497.

4 K. Saeedi, S. Simmons, J. Z. Salvail, P. Dluhy, H. Riemann, N. V. Abrosimov, P. Becker, H.–J. Pohl, J. J. L. Morton and M. L. W. Thewalt, Room–Temperature Quantum Bit Storage Exceeding 39 Minutes Using Ionized Donors in Silicon–28. *Science*, **2013**, *342*, 830–833.

5 Koch, J.; Yu, T. M.; Gambetta, J.; Houck, A. A.; Schuster, D. I.; Majer, J.; Devoret, M. H.; Girvin, S. M.; Schoelkopf, R. J. Charge–insensitive qubit design derived from the Cooper pair box. *Phys. Rev. A* **2007**, *76,* 042319.

6 (a) Wasielewski, M. R.; Forbes, M. D. E.; Frank, N. L.; Kowalski, K.; Scholes, G. D.; Baldo, M. A.; Freedman, D. E.; Goldsmith, R. E.; Goodson, T. III; Kirk, M. L.; McCusker, J. K.; Ogilvie, J. P.; Shultz, D. A.; Stoll, S.; Whaley, K. B.; Yuen-Zhou, J. Exploiting Chemistry and Chemical Systems for Quantum Information Science. *Nat. Rev. Chem.* **2020**, *4*, 490-504. (b) Sproules, S. Molecules as Electron Spin Qubits. *Electron Paramag. Reson.* **2017**, *25*, 61–97. (b) Luis, F.; Hill, S.; Coronado, E. Molecular Spins for Quantum Computation. *Nat. Chem.* **2019**, *11*, 301–309. (c) von Kugelgen, S.; Freedman, D. E. A chemical path to quantum information. *Science* **2019**, *366*, 1070- 1071.

7 (a) Yu, C.; Graham, M. J.; Zadrozny, J. M.; Niklas, J.; Krzyaniak, M. D.; Wasielewski, M. R.; Poluektov, O. G.; Freedman, D. E. Long Coherence Times in Nuclear Spin-Free Vanadyl Qubits. *J. Am. Chem. Soc.* **2016**, *138*, 14678-14685. (b) Graham, M. J.; Krzyaniak, M. D.; Wasielewski, M. R.; Freedman, D. E. Probing Nuclear Spin Effects on Electronic Spin Coherence via EPR Measurements of Vanadium(IV) Complexes. *Inorg. Chem.* **2017**, *56*, 8106-8113. (c) Graham, M. J.; Zadrozny, J. M.; Shiddiq, M.; Anderson, J. S.; Fataftah, M. S.; Hill, S.; Freedman, D. E. Influence of Electronic Spin and Spin-Orbit Coupling on Decoherence in Mononuclear Transition Metal Complexes. *J. Am. Chem. Soc.* **2014**, *136*, 7623-7626.

8 (a) Olshansky, J. H.; Kryaniak, M. D.; Young, R. M.; Wasielewski, M. R. Photogenerated Spin-Entangled Qubit (Radical) Pairs in DNA Hairpins: Observation of Spin Delocalization. *J. Am. Chem. Soc.*, **2019** *141*, 2152-2160. (b) Wu, Y.; Zhou, J.; Nelson, J. N.; Young, R. M.; Krzyaniak, M. D.; Wasielewski, M. R. Covalent Radical Pairs as Spin Qubits: Influence of Rapid Electron Motion between Two Equivalent Sites on Spin Coherence. *J. Am. Chem. Soc.*, **2018** *140*, 13011-13021. (c) Nelson, J. N.; Krzyaniak, M. D.; Horwitz, N. E.; Rugg. B. K.; Phelan, B. T.; Wasielewski, M. R. Zero Quantum Coherence in a Series of Covalent Spin-Correlated Radical Pairs. *J. Phys. Chem. A* **2017**, *121*, 2241-2252. (d) Yoshina, T.; Nishida, S.; Sato, S.; Nakazawa, S.; Rahimi, R. D.; Toyota, K.; Shiomi, D.; Morita, Y.; Kitagawa, M.; Takui, T.

ESR and ^{1}H-, ^{19}F-ENDOR/TRIPLE Study of Fluorinated Diphenylnitroxides as Synthetic Bus Spin-Qubit Radicals with Client Qubits in Solution. *J. Phys. Chem. Lett.* **2011**, *2*, 449-453. (e) Nakazawa, S.; Nishida, S.; Ise, T.; Yoshino, T.; Mori, N.; Rahimi, R. D.; Sato, K.; Morita, Y.; Toyota, K.; Shiomi, D.; Kitagawa, M.; Hara, H.; Carl, P.; Höfer, P.; Takui, T. A Synthetic Two-Spin Quantum Bit: G -Engineered Exchange-Coupled Biradical Designed for Controlled-NOT Gate Operations. *Agnew. Chem. Int. Ed.* **2012**, *51*, 9860–9864. (f) Sato, K.; Nakazawa, S.; Rahimi, R.; Ise, T.; Nishida, S.; Yoshino, T.; Mori, N.; Toyota, K.; Shiomi, D.; Yakiyama, Y.; Morita, Y.; Kitagawa, M.; Nakasuji, K.; Nakahara, M.; Hara, H.; Cark, P.; Höfer, P.; Takui, T. Molecular electron-spin quantum computers and quantum information processing: pulse-based electron magnetic resonance spin technology applied to matter spin-qubits. *J. Mater. Chem.* **2009**, *19*, 3739-3754. (g) McGuire, J.; Miras, H. N.; Donahue, J. P.; Richards, E.; Sproules, S. Ligand Radicals as Modular Organic Electron Spin Qubits. *Chem. Eur. J.* **2018**, *24*, 17598-17605.

9 Howe, M. E.; Garcia-Garibay, M. A. The Roles of Intrinsic Barriers and Crystal Fluidity on the Dynamics of Crystalline Molecular Rotors and Molecular Machines. *J. Org. Chem.* **2019**, *84*, 9835-9849.

10 Molecular rotation is currently being researched in a number of areas to create organic and hybrid materials with tunable and controllable properties: (a) Setaka, W.; Yamaguchi, K. Order-Disorder Transition of Dipolar Rotor in a Crystalline Molecular Gyrotop and Its Optical Change. *J. Am. Chem. Soc.* **2013**, *135*, 14560-14563. (b) Tsurunaga, M.; Inagaki, Y.; Momma, H.; Kwon, E.; Yamaguchi, K.; Yoza, K.; Setaka, W. Dielectric Relaxation of Powdered Molecular Gyrotops Having a Thiophene Dioxide-diyl as a Dipolar Rotor. *Org. Lett.* **2018**, *20*, 6934-6937. (c) Hashimoto, H.; Inagaki, Y.; Momma, H.; Kwon, E.; Setaka, W. Kinetic Stabilization of Carbazole Nitroxides by Inclusion in a Macrocage and Their Electron Spin Resonance Characterization. *J. Org. Chem.* **2019**, *84*, 11783-11789. (d) Masuda, T.; Arase, J.; Inagaki, Y.; Kawahata, M.; Yamaguchi, K.; Ohhara, T.l Nakao, A.; Momma, H.; Kwon, E.; Setaka, W. Molecular Gyrotops with a Five-Membered Heteroaromatic Ring: Synthesis, Temper-Dependent Orientation of Dipolar Rotors inside the Crystal and its Birefringence Change. *Cryst.Growth Des.* **2016**, *16*, 4392-4401. (e) Winston, E. B.; Lowell, P. J.; Vacek, J.; Chocholoušová, J.; Michl, J.; Price, J. C. Dipolar molecular rotors in the metal-organic framework crystal IRMOF-2. *Phys. Chem. Chem. Phys.* **2008**, *10*, 5188-5191. (f) Horinek, D.; Michl. J. Molecular Dynamics Simulation of an Electric Field Driven Dipolar Molecular Rotor Attached to a Quartz Glass Surface. *J. Am. Chem. Soc.* **2003**, *39*, 11900-11910. (g) Vacek, J.; Michl, J. Molecular dynamics of a grid-mounted molecular dipolar rotor in a rotating electric field. *PNAS* **2001**, *98*, 5481-5486. (h) Jin, M.; Yamamoto, S.; Seki, T.; Ito, H.; Garcia-Garibay, M. A. Anisotropic Thermal Expansion as the Source of Macroscopic and Molecular Scale Motion in Phosphorescent Amphidynamic Crystals. *Angew. Chem. Int. Ed.* **2019**, *58*, 18003-18010. (i) Colin-Molina, A.; Karothu, D. P.; Jellen, M. J.; Toscano, R. A.; Garcia-Garibay, M. A.; Naumov, P.; Rodriguez-Molina, B. "Thermosalient Amphidynamic Molecular Machines: Motion at the *Matter* Molecular and Macroscopic Scales. **2019**, *1*, 1033-1046.

11 (a) Graham, M. J.; Zadrozny, J. M.; Fataftah, M. S.; Freedman, D. E. Forging Solid-State Qubit Design Principles in a Molecular Furnace. *Chem. Mater.* **2017**, *29*, 1885-1897. (b) Urtizberea, A.; Natividad, E.; Alonso, P. J.; Andrés, M. J.; Gascón, I.; Goldmann, M.; Roubeau, O. A Porphyrin Spin Qubit and Its 2D Framework Nanosheets. *Adv. Funct. Mater.* **2018**, *28*, 1801695.

12 Yu, C.–J.; Krzyaniak, M.; Fataftah, M. S.; Wasielewski, M. R.; Freedman, D. E. A Concentrated Array of Copper Porphyrin Candidate Qubits. *Chem. Sci.* **2019**, *10*, 1702–1708.

13 Zadrozny, J. M.; Gallagher, A. T.; Harris, T. D.; Freedman, D. E. A Porous Array of Clock Qubits. *J. Am. Chem. Soc.* **2017**, *139*, 7089–7094.

14 T. Yamabayashi; M. Atzori; L. Tesi; G. Cosquer; F. Santanni; M.–E. Boulon; E. Morra; S. Benci; R. Torre; M. Chiesa Scaling Up Electronic Spin Qubits into a Three–Dimensional Metal–Organic Framework. *J. Am. Chem. Soc.* **2018**, *140*, 12090 –12101.

15 (a) Faust, T. B.; D'Alessandro, D. M. Radicals in metal-organic frameworks. *RSC Adv.* **2014**, *4*, 17498-17512. (b) Zwoliński, K. M.; Chmielewski, M. J. Tempo-Appended Metal-Organic Frameworks as Highly Active, Selective, and Mild Reusable Catalysts for Mild Aerobic Oxidation of Alcohols. *ACS Applied Materials & Interfaces* **2017**, *9*, 33956-33967 (c) Souto, M.; Strutynski, K.; Melle-Franco, M.; Rocha, J. Electroactive Organic Building Blocks for the Chemical Design of Functional Porous Frameworks (MOFs and COFs) in Electronics. *Chem. Eur. J.* **2020**, *26*, 10912-10935.

16 Vogelsberg, C. S.; Uribe–Romo, F. J.; Lipton, A. S.; Yang, S.; Houk, K. N.; Brown, S. Ultrafast Rotation in an Amphidynamic Crystalline Metal Organic Framework. *PNAS*, **2017**, *114*, 13613–13618.

17 Vacek, J.; Michl, J. Molecular dynamics of a grid-mounted molecular dipolar rotor in a rotating electric field. *Proc. Nat. Acad. Sc*. **2001**, *98*, 5481–5486.

18 DeLeeuw, S. W.; Solvaeson, D.; Ratner, M. A.; Michl, J. Molecular dipole chains: Excitations and dissipation. *J. Phys. Chem. B*., **1998**, *102*, 3876–3885.

19 (a) Chiarelli, R.; Novakt, M. A.; Rassat, A.; Tholencet, J. L. A Ferromagnetic Transition At 1.48 K in an Organic Nitroxide. *Nature* **1993**, *363*, 147–149. (b) You, A.; Be, M. A. Y.; Ferromagnetic and Antiferromagnetic Intermolecular Interactions of Organic Radicals, α– Nitronyl Nitroxides. II. *J. Chem. Phys.* **1989**, *91*, 2743.

20 Gauyacq, J. P. & Lorente, N. Extremely long–lived magnetic excitations in supported Fe chains. *Physical Review B*, **2016**, *94*, 045420.

21 Li, L.; Matsuda, R.; Tanaka, I.; Sato, H.; Kanoo, P.; Jeon, H.J.; Foo, M.W.; Wakamiya, A.; Murata, Y.; Kitagawa, S., A Crystalline Porous Coordination Polymer Decorated with Nitroxide Radicals Catalyzes Aerobic Oxidation of Alcohols. *J. Am. Chem. Soc.* **2014**, *136*, 7543–7546

22 Bajpai, A.; Lusi, M.; Zaworotko, M. J. The role of weak interactions in controlling the mode of interpenetration in hybrid ultramicroporous materials. *Chem. Commun.*, **2017**, *53,* 3978–3981 (b) Vagin, S. I.; Ott, A. K.; Hoffmann, S. D.; Lanzinger, D.; Rieger, B. Synthesis and Properties of (Triptycenedicarboxylato)Zinc Coordination Networks. *Chem. Eur. J.* **2009**, *15*, 5845–5853.

23 Jiang, X.; Duan, H–B.; Kahn, S.; Garcia–Garibay, M.A. Diffusion–Controlled Rotation of Triptycene in a Metal–Organic Framework (MOF) Sheds Light on the Viscosity of MOF–Confined Solvent. *ACS Cent. Sci*. **2016**, *2*, 608–613

24 Yuan, S.; Feng, L.; Wang, K.; Pang, J.; Bosch, M.; Lollar, C.; Sun, Y.; Qin, J.; Yang, X.; Zhang, P.; Wang, Q.; Zou, L.; Zhang, Y.; Zhang, L.; Fang, Y.; Li, J.; Zhou, H. Stable Metal – Organic Frameworks : Design, Synthesis, and Applications. *Adv. Mater.* **2018**, *30*, 1–35.

25 (a) Matsumoto, S.; Higashiyama, T.; Akutsu, H.; Nakatsuji, S. A Functional Nitroxide Radical Displaying Unique Thermochromism and Magnetic Phase Transition. *Angew. Chem. Int. Ed*., **2011**, *50*, 10879-10883. (b) Hoshino, N.; Takeda, T.; Akutagawa, T. Multifunctional Molecular Rotators with Dielectric Magnetic and Optical Responses. *RSC Adv*. **2014**, *4*, 743-747.

26 West, A. R. *Solid State Chemistry and its Applications, 2nd edition*; John Wiley & Sons: Chichester, 2014.

27 Oshio, H.; Watanabe, T.; Ohto, A.; Ito, T.; Masuda, H. Intermolecular Ferromagnetic and Antiferromagnetic Interactions in Halogen–Bridged Copper (I) Imino Nitroxides : Crystal Structures and Magnetic Properties of [Cu I (μ –X)(Imino Nitroxide)] 2 (X) I or Br). *Inorganic Chemistry* **1996**, *35*, 472–479.

28 Abdrakhmanov, R. S.; Garif'yanov, N. S.; Semenova, E. I. An EPR Study of Various Compounds of Copper (II) and Silver (II). *Theoretical and Experimental Chemistry* **1971**, *4*, 250–254.

29 Bales, B. L.; Meyer, M.; Peric, M. EPR Line Shifts and Line Shape Changes Due to Heisenberg Spin Exchange and Dipole–Dipole Interactions of Nitroxide Free Radicals in Liquids: 9. An Alternative Method to Separate the Effects of the Two Interactions Employing 15N and 14N. *The Journal of Physical Chemistry A **2014**, 118*, 6154–6162.

30 (a) Graham, M. J.; Yu, C.; Krzyaniak, M.; Wasielewski, M.; Freedman, D. E. Synthetic Approach to Determine the Effect of Nuclear Spin Distance on Electronic Spin Decoherence. *J. Am. Chem. Soc.* **2017**, *139*, 3196–3201. (b) Jeschke, G. Distance Measurements in the Nanometer Range by Pulse EPR. *Chem. Phys. Chem.* **2002**, *3*, 927–932.

31 Junk, M. J. N. Electron Paramagnetic Resonance Theory. *Assessing the Functional Structure of Molecular Transporters by EPR Spectroscopy*; Springer Berlin Heidelberg: Mainz 2012.

32 (a) Birrell, G. B.; Pong, S.; Griffith, V. & O.H. Electron Spin Resonance of Spin Labels in Organic Inclusion Crystals. Models for Anisotropic Motion in Biological Membranes. *J. Am. Chem. Soc.* **1973**, *95*, 2451–2458. (b) Kobayashi, H.; Ueda, T.; Miyakubo, K.; Eguchiab, T.; Tanib, A. ESR Study of Molecular Dynamics and Orientation of TEMPO Included in Organic 1-D Nanochannel, *Phys.Chem.Chem.Phys*. **2008**, *10*, 1263–1269.

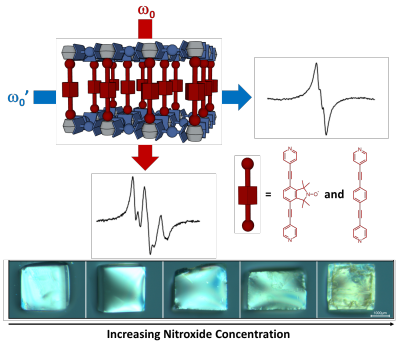
ω0
ω0'
=
and
Increasing Nitroxide Concentration